Journal of Materials Chemistry C

Accepted Manuscript

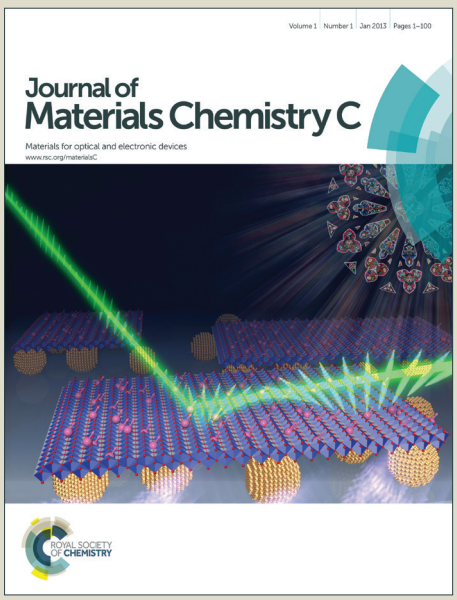

This is an *Accepted Manuscript*, which has been through the Royal Society of Chemistry peer review process and has been accepted for publication.

Accepted Manuscripts are published online shortly after acceptance, before technical editing, formatting and proof reading. Using this free service, authors can make their results available to the community, in citable form, before we publish the edited article. We will replace this *Accepted Manuscript* with the edited and formatted *Advance Article* as soon as it is available.

You can find more information about *Accepted Manuscripts* in the Information for Authors.

Please note that technical editing may introduce minor changes to the text and/or graphics, which may alter content. The journal's standard Terms & Conditions and the Ethical guidelines still apply. In no event shall the Royal Society of Chemistry be held responsible for any errors or omissions in this *Accepted Manuscript* or any consequences arising from the use of any information it contains.

ROYAL SOCIETY OF CHEMISTRY

www.rsc.org/materialsC

Journal of Materials Chemistry C

ARTICLE

Fabrication of thermoelectric materials - Thermal stability and repeatability of achieved efficiencies

Received 00th January 20xx,
Accepted 00th January 20xx

DOI: 10.1039/x0xx00000x

www.rsc.org/

S. Aminorroaya Yamini*[a] M. Brewis[a], J. Byrnes, R. Santos[a] , A. Manettas[a] and Y.Z. Pei[b]

Metal chalcogenides have delivered the highest efficiencies among thermoelectric materials. Although the thermal stability of thermoelectric materials at device operating temperatures has been of concern, recent studies have reported the efficiencies of materials prepared with different fabrication techniques. Here, we have fabricated a p-type, multiphase lead chalcogenide compound of $(PbTe)_{0.55}(PbS)_{0.35}(PbSe)_{0.1}$, with three common fabrication techniques of quenched, quenched-annealed and furnace cooled followed by spark plasma sintering. The compound contains PbS-rich precipitates within a PbTe-rich matrix. The achieved samples from various fabrication procedures demonstrate distinct microstructures that evolve with thermal cycling. We have shown that the thermoelectric efficiency of metastable compound is irreversible during thermal cycling, and changes by only three thermal cycles during measurements. Our findings highlight the importance of the choice of fabrication and post-processing techniques for thermoelectric materials.

Introduction

Solid-state thermoelectric generators, which convert heat to electricity, have attracted considerable attention for waste heat recovery [1]. Tremendous efforts have been denoted to improve the relatively low conversion efficiency of thermoelectric materials. The efficiency is defined by the dimensionless figure of merit, $zT = S^2T\sigma/(\kappa_E + \kappa_L)$, where, S, σ, T, κ_L, and κ_E are the Seebeck coefficient, electrical conductivity, absolute temperature, and the lattice and electronic components of the thermal conductivity, respectively.

Bulk metal chalcogenides have provided the highest efficiencies amongst thermoelectric materials [2-6]. Recently, thermoelectric properties of polycrystalline materials have been measured in samples that are only quenched from the melt [7, 8], sintered (powder metallurgy) directly from quenched samples without annealing [4, 9-12], or furnace cooled from the melt to room temperature followed by powder sintering [11, 13, 14]. However, polycrystalline bulk thermoelectric metal chalcogenides were traditionally fabricated through homogenising of stoichiometric ratios of elements at the liquid phase, followed by rapid cooling to room temperature, and finally annealing the compound [15]. An improvement in the mechanical properties of thermoelectric materials was reported when the obtained ingot from casting techniques were reprocessed by powder metallurgy [4, 15]. This includes powdering the ingot and sintering under hydrostatic pressure at elevated temperatures [15]. The quenched samples (either in water, salt water or liquid nitrogen) [7, 16] or sintered pellets from quenched samples [4, 9], frequently demonstrate higher thermoelectric efficiencies than annealed ones. Therefore, the respected fabrication methods occasionally have been introduced as an effective technique to improve the efficiency of thermoelectric materials [7, 9, 16]. Nevertheless, there is no report available on reproducibility of the obtained transport properties of these samples.

In addition, nanostructuring of bulk materials through nucleation and growth of precipitates [17, 18] or transformations [4, 8, 19], results in low lattice thermal conductivity [20, 21] and consequently improves the figure of merit of thermoelectric materials. Although a high zT has been reported for these compounds, their stability at the operating temperatures in thermoelectric generators needs to be studied, due to the high thermodynamic driving forces within these materials to eliminate the interfaces [22, 23].

Here, we have explored the thermoelectric properties and reproducibility of the results, for a phase-separated p-type quaternary $(PbTe)_{0.55}(PbS)_{0.35}(PbS)_{0.1}$ compound prepared by various fabrication techniques. Phase separated, nanostructured, p-type ternary lead chalcogenides have demonstrated high thermoelectric efficiencies, [13, 24] and quaternary lead chalcogenides have provided superior

[a] Australian Institute for Innovative Materials, University of Wollongong, North Wollongong, NSW 2500, Australia.
[b] School of Materials Science and Engineering, Tongji University, 4800 Caoan Road, Shanghai 201804, China.
† Corresponding author: Dr. Sima Aminorroaya Yamini. Sima@uow.edu.au.
Electronic Supplementary Information (ESI) available: [details of any supplementary information available should be included here]. See DOI: 10.1039/x0xx00000x

This journal is © The Royal Society of Chemistry 20xx

Journal of Materials Chemistry C Accepted Manuscript

Please do not adjust margins

Please do not adjust margins

thermoelectric efficiencies to the binary and ternary systems [25, 26]. We have adopted three common preparation routes to fabricate the compounds. The stoichiometric ratio of elements were homogenized in liquid phase and; (i) quenched in water (Q); (ii) quenched in water followed by annealing (QA), and (iii) furnace cooled to room temperature (FC). All samples were sintered using the Spark Plasma Sintering (SPS) technique, with identical conditions used for all samples. We have shown that the thermoelectric efficiency of a quenched sample (Q) is higher than thermally stable specimens in the first round of measurement, then reduces during thermal cycling to approach the efficiency of thermally stable samples. It is explained by the growth of precipitates and microstructural evolution of compounds during thermal cycling.

Experimental

Sample fabrication

Synthesis: A polycrystalline PbS sample was prepared by mixing high purity Pb (99.999%) and dried S (99.9%) in vacuum sealed quartz ampoules, then reacted at high temperature to produce high purity PbS starting material. The final polycrystalline $Pb_{0.97}Na_{0.03}Te_{0.55}S_{0.35}Se_{0.1}$ samples were synthesized by mixing stoichiometric quantities of high purity PbS, Se, Pb, Te and Na as the dopant. A total mass of 10 g was sealed in carbon-coated quartz tubes under vacuum, and then heated to 1373 K followed by homogenizing at that temperature for 10 hours. Two samples were quenched in cold water. One was transferred directly to the sintering procedure (Q), the other annealed at 823 K for 72 hours (QA). A sample was cooled in the furnace from the homogenized melt (FC). The chemistry of all three samples was identical and sodium was selected as *p*-type dopant.

Sintering: The resulting ingots from the synthesis procedure were hand-ground to powder with an agate mortar and pestle. The powders were sintered into 12 mm diameter disk-shaped pellets using spark plasma sintering (SPS) at 773 K and an axial pressure of 40 MPa for an hour under vacuum.

Transport properties measurements

Seebeck coefficient and resistivity measurements: The pressed samples were cut and polished into parallelepipeds. The electrical conductivity and Seebeck coefficient were measured using a Linseis LSR-3 instrument. Samples were held between two tungsten electrodes and two probe thermocouples with spring-loaded pressure contacts. Measurements were made under 0.1 atm of helium and were collected from room temperature to 850 K.

Thermal conductivity measurements: The thermal conductivity (κ) was calculated from $\kappa = \rho D_T C_p$. The laser flash method (Linseis LFA 1000) was used to measure the thermal diffusivity (D_T), and the density (ρ) was calculated using the measured weight and dimensions. The specific heat capacity (C_p), was estimated by $Cp(k_B$ per atom) = 3.07 + 4.7 × 10^{-4} × (T(/K) − 300) [27], that is believed to be accurate for lead chalcogenides [3, 4]. The combined uncertainty for all measurements involved in *z*T determination is ~ 20% [28].

Hall measurements: Samples were loaded onto a heated BN substrate and four probes were attached to the edge of the sample. The sample was placed in a vacuum with a magnetic field (up to ± 1.5 T) perpendicular to its surface. The resistivity (ρ) and Hall coefficient (R_H) (perpendicular to the hot-pressing direction) were measured using the van de Pauw method

Materials characterisation

X-Ray Diffraction: The crystallographic structure and composition were characterized by X-Ray Diffraction (XRD) using a GBC Scientific X-ray diffractometer with Cu K_α radiation (λ = 1.544 Å, 40 kV, 25 mA). The phase ratio and lattice parameters were calculated from the X-ray diffraction patterns using Rietveld analysis.

Electron Microscopy Analyses: Samples were characterized using a JEOL 7001 scanning electron microscope (SEM). SEM samples were prepared by polishing to a quarter of micron final finish.

Results and discussion

XRD analysis

The microstructure of the quaternary PbTe-PbSe-PbS system is similar to the ternary PbTe-PbS compounds, due to unlimited solubility of PbTe and PbS in PbSe, and the presence of only a miscibility gap in the PbTe-PbS ternary system [29]. Alloying of PbS beyond its solubility limit, results in PbS-rich precipitates within the PbTe-rich matrix, with a NaCl-type Face Centred Cubic (FCC) crystal structure [30]. The current study compound of $(PbTe)_{0.55}(PbS)_{0.35}(PbSe)_{0.1}$ can be simplified as PbTe, which is initially alloyed with 10 at% PbSe to form a solid solution parent compound of $(PbTe)_{0.9}(PbSe)_{0.1}$. This is then further alloyed with PbS beyond its solubility limit (~8 at. %) to form PbS-rich precipitates in the PbTe-rich matrix [30]. Both the PbS-rich precipitates and PbTe-rich matrix have a NaCl-type face centred cubic (FCC) crystal structure [29]. The XRD patterns obtained from cast samples in **Figure 1(a),** show that the FC and QA samples contain both PbS-rich and PbTe-rich phases, whereas the Q sample reveals a single phase. The XRD patterns obtained from sintered specimens fabricated from cast samples by SPS in **Figure 1(b),** revealed two phases indicating that phase separation occurred for the Q sample during sintering. The Rietveld refinement was employed to determine the phase ratio and the lattice parameters of the phases by extrapolating from high angle diffraction peaks. The results show 26.9± 2.5 wt% precipitates in the matrix for all sintered samples. The lattice parameter of the matrices (a = 6.4± 0.02 Å) is smaller than for pure PbTe (a = 6.46 Å), indicating that the PbTe-rich matrix is alloyed with PbSe (a = 6.13 Å) and PbS (a = 5.93 Å), where both phases possess smaller lattice parameters. The lattice parameter of the precipitates (a = 5.96± 0.01 Å) is larger than that of pure PbS,

Journal of Materials Chemistry C Accepted Manuscript

This journal is © The Royal Society of Chemistry 20xx

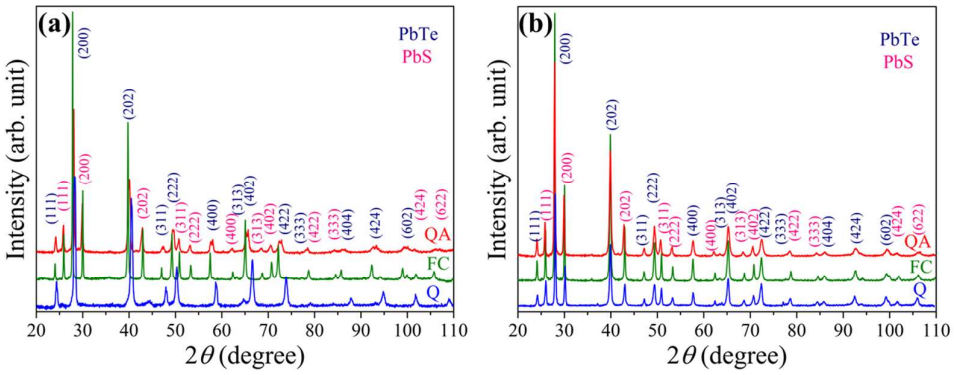

Figure 1. Room temperature X-ray diffraction patterns for (a) cast, (b) sintered samples of quenched (Q), quenched and annealed (QA) and furnace cooled (FC) of $Pb_{0.97}Na_{0.03}Te_{0.55}S_{0.35}Se_{0.1}$ compounds.

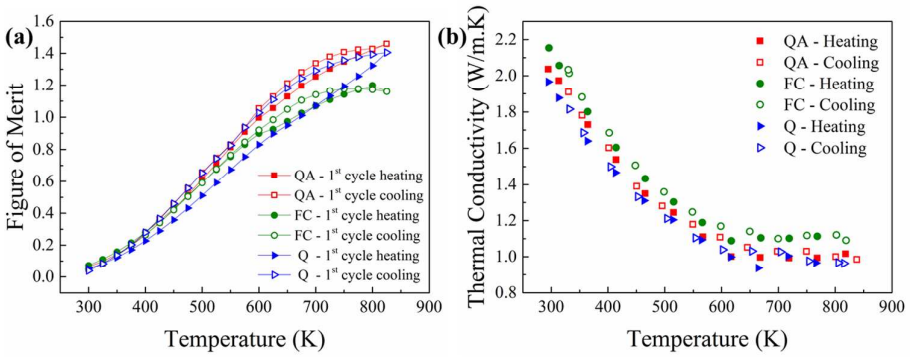

Figure 2. Temperature dependent (a) Figure of merit (zT), (b) measured total thermal conductivity, κ (W/m·K), of sodium-doped $(PbTe)_{0.55}(PbS)_{0.35}(PbSe)_{0.1,}$ sintered bulk samples fabricated by quenching (Q), quenching followed by annealing (QA) and furnace cooling from the melt (FC) during heating and cooling.

which, indicates solubility of PbTe and PbSe in the precipitates as expected from the phase diagram [29]. The average crystallite size for the matrix and precipitates were calculated from the full width at half maximum (FWHM) of the reflected peaks in Figure 1(b) using Williamson-Hall plot. This method can also be used to determine the dislocation density [31]. The results are discussed in Supporting Information.

Transport properties measurements

Figure 2(a) shows the temperature dependent thermoelectric efficiencies of Na-doped $(PbTe)_{0.55}(PbS)_{0.35}(PbSe)_{0.1}$ samples prepared by various fabrication techniques. Although the chemical composition of all samples is identical, their thermoelectric efficiencies vary by the fabrication technique. The Q and QA samples demonstrate a zT of ~ 1.5 whereas the maximum zT for the furnace cooled sample is ~1. There is also a substantial difference between the thermoelectric performances of the Q sample during the heating and cooling cycles. The total thermal conductivity of samples as a function of temperature in the range of 300-850 K in Figure 2(b), show no significant difference between the heating and cooling curves. Therefore the thermal conductivity of samples has no significant contribution to the variation of the thermoelectric performance of samples on heating and cooling. However, the Q sample has lower thermal conductivity than the QA and FC samples. This is in agreement with crystallite size analysis (detailed in **Supporting Information**), where the Q and FC samples show the smallest and largest crystallite sizes respectively. The room temperature thermal conductivities of Q and QA samples are approximately 2 W/m.K which is reduced to ~ 1 W/m.K above 600K. The thermal conductivity of the FC sample is reduced from ~2.2 W/m.K at room temperature to ~1.1 at temperatures above 600 K.

In order to study the thermal stability of samples, the transport properties measurements were repeated twice for every sample. **Figure 3(a to c)** show the Seebeck coefficients and **Figure 3(d to f)** demonstrate the electrical resistivities of Q, FC and QA samples as a function of temperature in the range of 300-850 K for three runs respectively. There are small variations between heating and cooling curves for Seebeck coeeficient values from the three runs of all samples. However, the differences are as small as measurement errors. **Figure 3(d to f)** clearly demonstrate the electrical resistivity variations between heating and cooling curves and also for three consecutive runs. The detailed information about repeated experiments for more samples and thermal cycles are summarised in **Supporting Information**.

Journal of Materials Chemistry C Accepted Manuscript

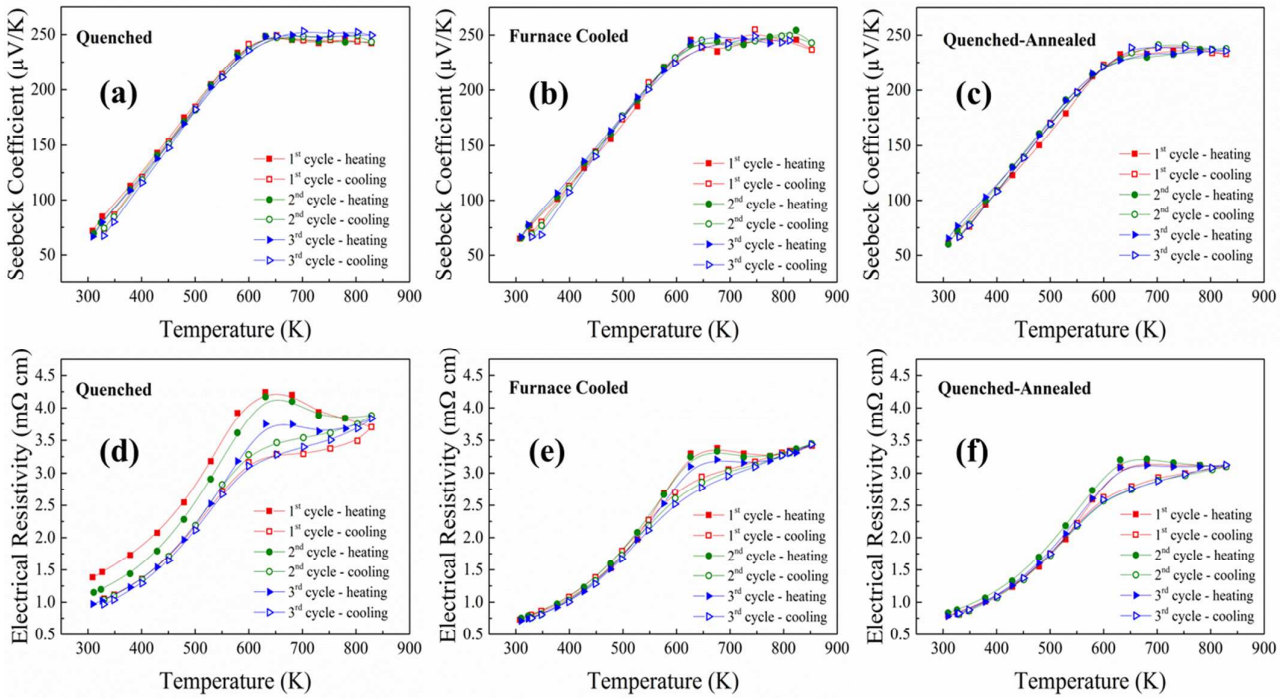

Figure 3. Temperature dependent Seebeck coefficient (μV/K) of (a) Q, (b) FC, (c) QA; and electrical resistivity (mΩ·cm) of (d) Q, (e) FC, (f) QA, sintered bulk sodium-doped $(PbTe)_{0.55}(PbS)_{0.35}(PbSe)_{0.1}$ samples.

There is a distinguished difference between the heating and cooling curves for the electrical resistivity from all samples. However, the results are reproducible for QA and FC samples. We [32] correlated this reproducible anomaly to the inhomogeneous distribution of sodium dopant between the matrix and secondary phase and its redistribution at high temperatures in the Na-doped multiphase lead-chalcogenide compounds. Conversely, the temperature dependant electrical resistivity values of the Q sample, are not only different between the heating and cooling curves, but also differ by thermal cycling.

The temperature dependent thermoelectric efficiencies of samples at the third run of measurements in **Figure 4,** show that the figure of merit for the Q sample, is decreased considerably compared to the first run (shown in Figure 2(a)), whereas the efficiency of QA and FC samples remain roughly the same after three thermal cycles. The room temperature Hall carrier concentrations ($n_H = r_H / e.R_H$) of the samples show that despite the intention of fabricating samples with identical carrier concentrations, the QA sample has a slightly higher carrier concentration of 9×10^{19} than 8.2×10^{19} for the Q and FC samples. This causes a lower electrical resistivity for the QA sample compared to the FC sample, which is in combination with lower lattice thermal conductivity results in higher thermoelectric efficiency for the QA sample than the FC sample. The electrical resistivity and Seebeck coefficient of all samples for three runs are compared in the **Supporting Information**. The difference between the thermoelectric efficiency of the QA and FC samples originates mainly from the difference in carrier concentrations. It is anticipated that the QA sample will provide a similar efficiency to the FC sample at similar carrier concentrations. Thermoelectric efficiency of Q sample at the first cycles is higher than FC sample with similar carrier concentration. However, the efficiency values of this sample are approaching to the efficiency of FC sample by thermal cycles. This indicates that the Q sample provides non-reproducible higher thermoelectric efficiency than the more thermally stable QA and FC samples at first cycles.

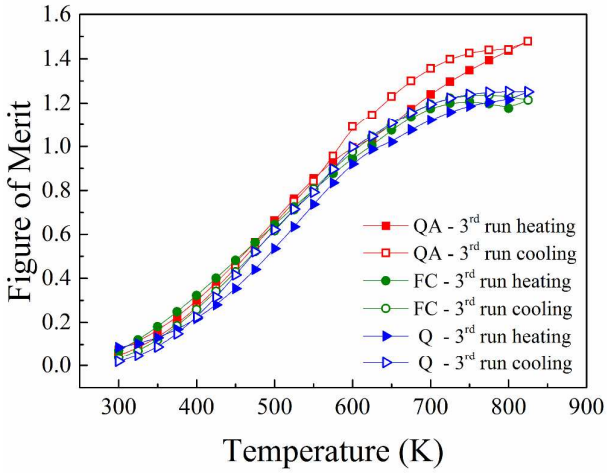

Figure 4. Temperature dependent Figure of merit of sodium-doped $(PbTe)_{0.55}(PbS)_{0.35}(PbSe)_{0.1,}$ sintered bulk samples fabricated by quenching (Q), quenching followed by annealing (QA) and furnace cooling from the melt (FC) during heating and cooling for the third measurement run.

This journal is © The Royal Society of Chemistry 20xx

Please do not adjust margins

Journal of Materials Chemistry C Accepted Manuscript

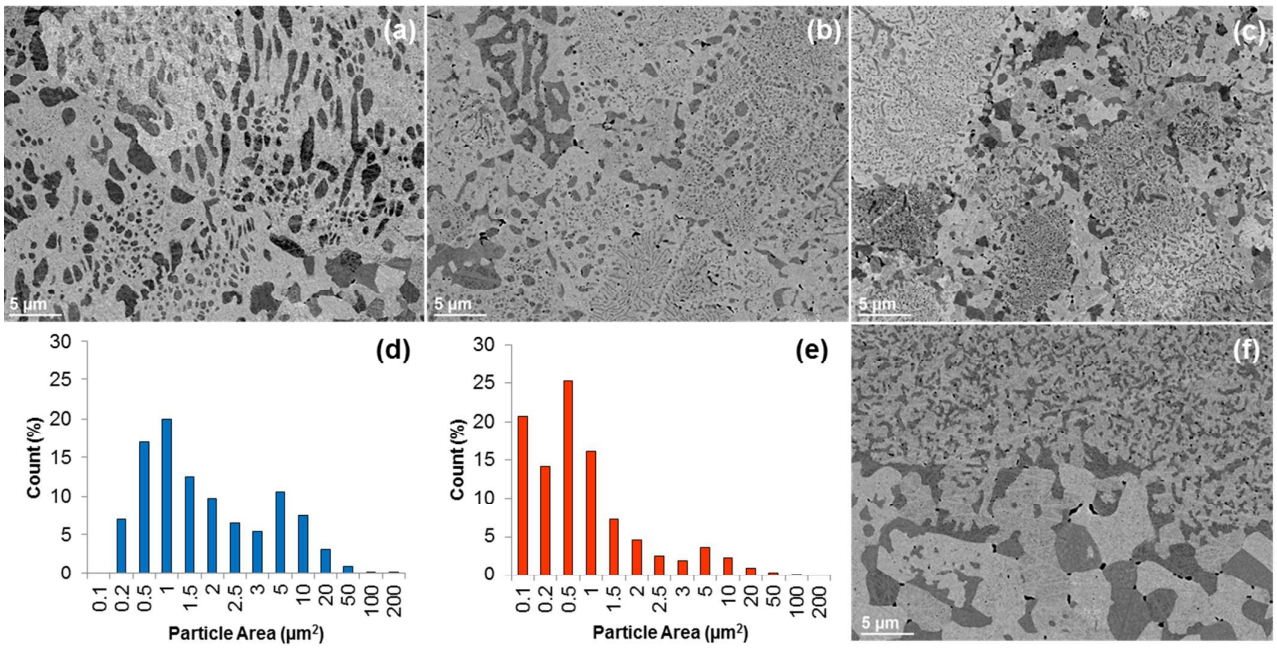

Figure 5.Typical SEM micrographs of sintered samples which were (a) furnace cooled, (b) annealed following quenching and (c) quenched in water; (d) and (e) show histogram based on particle area for the furnace cooled and annealed samples respectively; (f) SEM micrograph of the Q sample after three thermal cycles during transport properties measurement, indicating the precipitates size growth.

The detailed electron microscopy analysis was performed to evaluate the microstructure of samples prepared by various fabrication techniques and assess the possible effects on their transport properties. Transmission Electron Microscopy (TEM) is commonly employed to analyse the precipitates in similar compounds [8, 11, 33, 34]. In the current study, we have adopted high resolution Scanning Electron Microscopy (SEM) to assess the microstructural inhomogeneity of samples in larger area. **Figure 5(a to c)** show the SEM images of sintered FC, QA and Q sample respectively. Detailed composition analysis of the precipitates and matrix are discussed in the **Supporting Information**.

There are distinct differences between the size, morphology and distribution of precipitates in these samples. The FC sample contains more round precipitates that are on average, much larger in size than precipitates observed in either the QA or Q samples. The histogram of precipitate size distribution in samples FC and QA in **Figures 5 (d) and (e)** respectively, indicate that the FC sample contains a higher frequency of precipitates > 1 μm^2 than the annealed sample, while containing comparatively less precipitates below this size. Precipitates below 0.1 μm^2 were omitted from this analysis due to resolution limits of the used SEM micrographs. The morphology of precipitates in the QA sample shares similarities with the Q sample, with large distributions of areas containing fine precipitates, surrounded by larger, round precipitates. It suggests that precipitate growth at particle interfaces during sintering, has occurred much quicker than the inner particles. The fine precipitates in the QA sample are much larger than the ones in the Q sample due to precipitation and growth of PbS-rich precipitates during three days of annealing. XRD results in Figure 1, suggest that precipitation in the Q sample occurred only during sintering. Consequently, limited particle growth provides a much finer structure. It explains the lower thermal conductivity observed in **Figure 2(d)**.

Figure 5(f) demonstrates the inner grain structure of the Q sample after three thermal cycles of transport properties measurements at the same magnification of Figure 5(c). The average particle size appears to increase due to precipitate growth by thermal cycling. It suggests that even powder metallurgy of compounds is insufficient to provide a stable sample, although the XRD results show a similar secondary phase ratio and lattice parameters for all samples. The large variation in transport properties, more evident in the electric resistivity curves of the Q sample during measurements in as few as three thermal cycles, indicates that the metastable phases formed during quenching require appropriate post processing.

Conclusions

The multiphase *p*-type quaternary $(PbTe)_{0.55}(PbS)_{0.35}(PbS)_{0.1}$ compound was fabricated by quenching, quenching followed by annealing and cooling to room temperature in the furnace. All samples were subsequently sintered by the Spark Plasma Sintering (SPS) technique for an hour. The thermoelectric efficiency of the Q sample shows irreversible transport properties. Although the efficiency of the Q sample is higher than thermally stable specimens at the first measurement, it is

Journal of Materials Chemistry C Accepted Manuscript

Please do not adjust margins

reduced by thermal cycling, approaching the efficiency of more stable compounds. The FC sample exhibits the largest precipitate size, followed by the QA and Q samples. Despite the different morphology of precipitates in the QA and FC samples, the transport properties of both samples are reversible with thermal cycling. Our results indicate that precipitates also grow significantly in the Q sample with thermal cycles.

Although the thermal stability of nanostructured thermoelectric materials has been the scientists concern, reporting the highest thermoelectric efficiency values in materials has driven the focus of research. There are a number of high performance thermoelectric materials that have recently been reported with adherence to thermally unstable compositions and/or nanostructures. Our findings highlight the importance of the choice of fabrication and post-processing techniques of heterogeneous and/or nanostructured thermoelectric materials. Attention should also be focused on reproducibility of reported transport properties.

Acknowledgements

SAY would like to thank Australian Research Council (ARC) Discovery Early Career Award for financial support (DE130100310). The authors acknowledge use of facilities within the Electron Microscopy Centre, University of Wollongong.

Notes and references

1 L. E. Bell, Science, 2008, 321, 1457-1461.
2 S. Kim, K. H. Lee, H. A. Mun, H. S. Kim, S. W. Hwang, J. W. Roh, D. J. Yang, W. H. Shin, X. S. Li, Y. H. Lee, G. J. Snyder and S. W. Kim, Science, 2015, 348, 109-114.
3 Y. Pei, X. Shi, A. LaLonde, H. Wang, L. Chen and G. J. Snyder, Nature, 2011, 473, 66-69.
4 K. Biswas, J. He, I. D. Blum, C.-I. Wu, T. P. Hogan, D. N. Seidman, V. P. Dravid and M. G. Kanatzidis, Nature, 2012, 489, 414-418.
5 H. Liu, X. Shi, F. Xu, L. Zhang, W. Zhang, L. Chen, Q. Li, C. Uher, T. Day and G. J. Snyder, Nat Mater, 2012, 11, 422-425.
6 Y. Gelbstein, J. Davidow, S. N. Girard, D. Y. Chung and M. Kanatzidis, Adv. Energy Mater., 2013, 3, 815-820.
7 L.-l. Zhao, X.-l. Wang, J.-y. Wang, Z.-x. Cheng, S.-x. Dou, J. Wang and L.-q. Liu, Sci. Rep., 2015, 5, 7671.
8 J. He, S. N. Girard, J.-C. Zheng, L. Zhao, M. G. Kanatzidis and V. P. Dravid, Adv. Mater., 2012, 24, 4440-4444.
9 H. Wang, J.-H. Bahk, C. Kang, J. Hwang, K. Kim, J. Kim, P. Burke, J. E. Bowers, A. C. Gossard, A. Shakouri and W. Kim, Proc. Natl. Acad. Sci. U.S.A., 2014, 111, 10949-10954.
10 L.-D. Zhao, J. He, C.-I. Wu, T. P. Hogan, X. Zhou, C. Uher, V. P. Dravid and M. G. Kanatzidis, J. Am. Chem. Soc., 2012, 134, 7902-7912.
11 H. J. Wu, L. D. Zhao, F. S. Zheng, D. Wu, Y. L. Pei, X. Tong, M. G. Kanatzidis and J. Q. He, Nat Commun, 2014, 5.
12 L.-D. Zhao, S. Hao, S.-H. Lo, C.-I. Wu, X. Zhou, Y. Lee, H. Li, K. Biswas, T. P. Hogan, C. Uher, C. Wolverton, V. P. Dravid and M. G. Kanatzidis, J Am. Chem. Soc., 2013, 135, 7364-7370.
13 S. N. Girard, J. He, X. Zhou, D. P. Shoemaker, C. M. Jaworski, C. Uher, V. P. Dravid, J. P. Heremans and M. G. Kanatzidis, J. Am. Chem. Soc., 2011, 133, 16588-16597.
14 Q. Zhang, F. Cao, W. Liu, K. Lukas, B. Yu, S. Chen, C. Opeil, D. Broido, G. Chen and Z. Ren, J Am. Chem. Soc., 2012, 134, 10031-10038.
15 Y. I. Ravich, B. A. Efimova and I. A. Smirnov, Semiconducting lead chalcogenides Plenum Press in New York, 1970.
16 H. Wang, J. Hwang, M. L. Snedaker, I.-h. Kim, C. Kang, J. Kim, G. D. Stucky, J. Bowers and W. Kim, Chem. Mater., 2015, 27, 944-949.
17 Y. Pei, N. A. Heinz, A. LaLonde and G. J. Snyder, Energy Environ. Sci., 2011, 4, 3640-3645.
18 Y. Lee, S.-H. Lo, J. Androulakis, C.-I. Wu, L.-D. Zhao, D.-Y. Chung, T. P. Hogan, V. P. Dravid and M. G. Kanatzidis, J Am. Chem. Soc., 2013, 135, 5152-5160.
19 H. Wang, J.-H. Bahk, C. Kang, J. Hwang, K. Kim, J. Kim, P. Burke, J. E. Bowers, A. C. Gossard, A. Shakouri and W. Kim, Proceeding of the National Academy of Science of the United State of America, 2014, 111, 10949.
20 J. P. Heremans, M. S. Dresselhaus, L. E. Bell and D. T. Morelli, Nature Nanotechnology, 2013, 8, 471-473.
21 L.-D. Zhao, V. P. Dravid and M. G. Kanatzidis, Energy Environ. Sci., 2014.
22 P. A. Sharma and J. D. Sugar, Frontiers in Chemistry, 2014, 2, 111.
23 S. Gorsse, P. Bellanger, Y. Brechet, E. Sellier, A. Umarji, U. Ail and R. Decourt, Acta Mater., 2011, 59, 7425-7437.
24 D. Wu, L.-D. Zhao, X. Tong, W. Li, L. Wu, Q. Tan, Y. Pei, L. Huang, J.-F. Li, Y. Zhu, M. Kanatzidis and J. He, Energy Environ. Sci., 2015, 8, 2056-2068.
25 S. Aminorroaya Yamini, H. Wang, Z. Gibbs, Y. Pei, S. X. Dou and G. J. Snyder, Phys. Chem. Chem. Phys., 2014, 16, 1835-1840.
26 R. J. Korkosz, T. C. Chasapis, S.-h. Lo, J. W. Doak, Y. J. Kim, C.-I. Wu, E. Hatzikraniotis, T. P. Hogan, D. N. Seidman, C. Wolverton, V. P. Dravid and M. G. Kanatzidis, J Am. Chem. Soc., 2014, 136, 3225-3237.
27 A. S. Pashinkin, M. S. Mikhailova, A. S. Malkova and V. A. Fedorov, Inorg. Mater., 2009, 45, 1226-1229.
28 K. A. Borup, J. de Boor, H. Wang, F. Drymiotis, F. Gascoin, X. Shi, L. Chen, M. I. Fedorov, E. Muller, B. B. Iversen and G. J. Snyder, Energy Environ. Sci., 2014, 8, 423-435.
29 A. Volykhov, L. Yashina and V. Shtanov, Inorg. Mater., 2010, 46, 464-471.
30 S. Aminorroaya Yamini, H. Wang, Z. Gibbs, Y. Pei, David Mitchel, S. X. Dou and G. J. Snyder, Acta Mater., 2014, 80, 365-372.
31 K. Zhang, S. J. Kim, Y. Zhang, T. Heeg, D. G. Schlom, W. Shen and X. Pan, J. Phys. D: Appl. Phys., 2014, 47, 105302.
32 S. Aminorroaya Yamini, David Mitchel, H. Wang, Z. Gibbs, Y. Pei, S. X. Dou and G. J. Snyder, AIP Advances, 2014, 5, 053601.
33 J. He, I. D. Blum, H.-Q. Wang, S. N. Girard, J. Doak, L.-D. Zhao, J.-C. Zheng, G. Casillas, C. Wolverton, M. Jose-Yacaman, D. N. Seidman, M. G. Kanatzidis and V. P. Dravid, Nano Lett., 2012, 12, 5979-5984.
34 J. He, S. N. Girard, M. G. Kanatzidis and V. P. Dravid, Adv. Funct. Mater., 2010, 20, 764-772.

Journal of Materials Chemistry C Accepted Manuscript

This journal is © The Royal Society of Chemistry 20xx

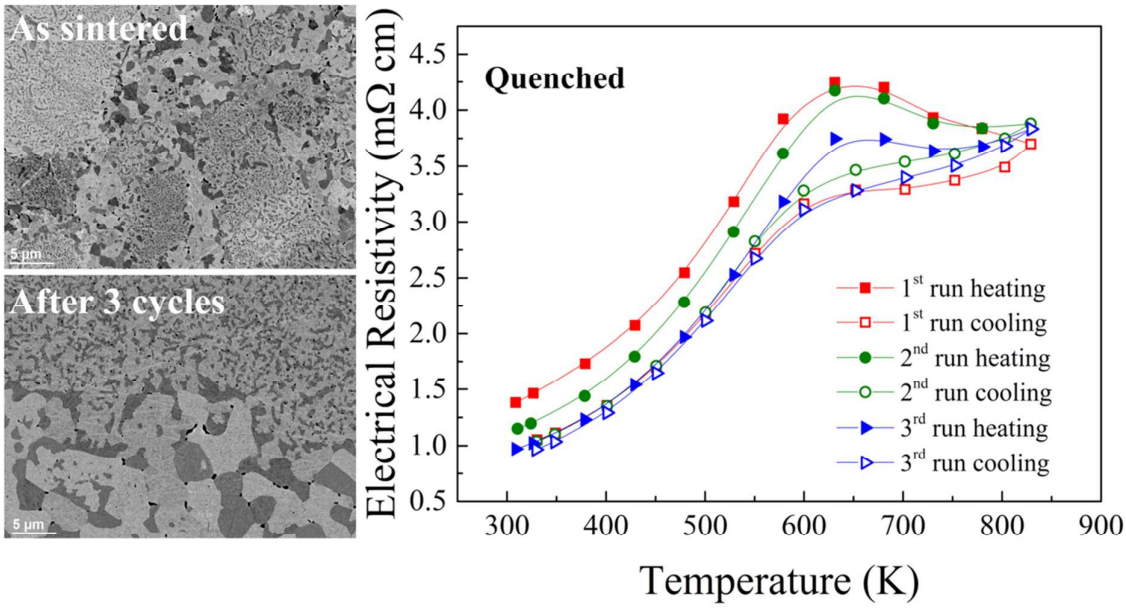

Thermoelectric properties of metastable PbTe-based thermoelectric material degrade with thermal cycling.

Journal of Materials Chemistry C Accepted Manuscript